J Comput Electron (2016) 15:76–83
DOI 10.1007/s10825-015-0755-4

CrossMark

A simulation study of short channel effects with a QET model based on Fermi–Dirac statistics and nonparabolicity for high-mobility MOSFETs

Shohiro Sho[1] · Shinji Odanaka[1] · Akira Hiroki[2]

Published online: 7 October 2015
© The Author(s) 2015. This article is published with open access at Springerlink.com

Abstract In this paper, the quantum confinement and short channel effects of Si, Ge, and $In_{0.53}Ga_{0.47}As$ n-MOSFETs are evaluated. Both bulk and double-gate structures are simulated using a quantum energy transport model based on Fermi–Dirac statistics. Nonparabolic band effects are further considered. The QET model allows us to simulate carrier transport including quantum confinement and hot carrier effects. The charge control by the gate is reduced in the Ge and $In_{0.53}Ga_{0.47}As$ bulk n-MOSFETs due to the low effective mass and high permittivity. This charge control reduction induces the degradation of short channel effects. In double-gate structures, different improvements of drain induced barrier lowering (DIBL) and subthreshold slope (SS) are seen. The double-gate structure is effective in the suppression of DIBL for all channel materials. The SS degradation depends on channel materials even in double-gate structure.

Keywords Quantum energy transport (QET) model · Nonparabolic band effects · Fermi–Dirac statistics · Quantum confinement · Short channel effects · $In_{0.53}Ga_{0.47}As$

1 Introduction

The scaling of conventional bulk Si-MOSFET approaches the fundamental limit due to the increase of off-leakage current and short channel effects [1]. Further performance improvements require new channel materials such as Ge and III–V compound semiconductors [2] and new device structures such as FinFETs [3] and nanowire gate-all-around structures [4]. Performance analysis of single and multi-gate MOSFETs on high mobility substrates and Si is an important issue. A number of authors have focused on numerical and theoretical studies of such devices, using self-consistent Poisson/Monte Carlo simulations [5,6], comprehensive semiclassical multisubband Monte Carlo simulations [7], self-consistent solutions of Schrödinger/Poisson equations [6,8,9], a quantum-corrected Monte Carlo simulations [10], and an atomistic Schrödinger/Poisson equations in the non-equilibrium Green's function formalism [11].

This paper describes performance analysis of Si, Ge, and $In_{0.53}Ga_{0.47}As$ n-MOSFETs using a quantum energy transport (QET) model based on Fermi–Dirac statistics and nonparabolicity. The QET model is viewed as one of the hierarchy of the quantum hydrodynamic models [12], which allows simulations of carrier transport including quantum confinement and hot carrier effects [13]. The simulation study focuses on the analysis of quantum confinement and short channel effects. Both bulk and double-gate n-MOSFETs are simulated.

The paper is organized as follows: In Sect. 2, we describe a four-moments QET model based on Fermi–Dirac statistics and nonparabolicity. Section 3 presents numerical simulations of the QET model. The results are further compared with those calculated by quantum drift diffusion (QDD) and classical energy transport (ET) models. The analysis of short channel and quantum confinement effects of Si, Ge, and $In_{0.53}Ga_{0.47}As$ n-MOSFETs for bulk and double-gate structures is presented. The dependence of short channel effects on channel materials is discussed. Section 4 concludes this paper.

✉ Shohiro Sho
shohiro@cas.cmc.osaka-u.ac.jp

1 Computer Assisted Science Division, Cybermedia Center, Osaka University, Toyonaka, Osaka 560-0043, Japan

2 Department of Electronics, Kyoto Institute of Technology, Kyoto, Japan

2 QET model

2.1 4-moments QET model based on Fermi–Dirac statistics

For the simulations of quantum confinement transport with hot carrier effects, we develop a four-moments QET model in [13]. This model is viewed as one of the hierarchy of the quantum hydrodynamic models [12]. In classical hydrodynamic simulations, a four-moments energy transport model is proposed in [14] for simulations of thin body MOSFETs. In this work, Fermi–Dirac statistics and nonparabolic corrections are further included for the performance analysis of MOSFETs on high mobility substrates. In fact, high mobility materials such as III–V compound semiconductors have strong degeneracy, low density of state, and nonparabolic band structures [15].

Numerical implementation of Fermi–Dirac statistics is discussed in [16] for QDD models and in [17] for QET models. The electron density n is approximated by introducing the band parameter ω_n as

$$n = n_i \exp\left(\frac{q}{kT_n}(\varphi + \gamma_n + \omega_n - \varphi_n)\right), \quad (1)$$

where φ, φ_n, and T_n are the electrostatic potential, quasi-Fermi-level, and electron temperature, respectively. n_i, q, and k are the intrinsic carrier density, electronic charge, and Boltzmann constant, respectively. The quantum potential γ_n is described as

$$\gamma_n = \frac{\hbar^2}{6mq}\frac{1}{\sqrt{n}}\frac{\partial^2}{\partial x_j^2}\sqrt{n}, \quad (2)$$

where m and $\hbar$ are the effective mass and Plank constant. The band parameter ω_n is determined as

$$\omega_n = \frac{kT_n}{q}\left(\log\left(\frac{n}{N_c}\right) - G_{\frac{1}{2}}\left(\frac{n}{N_c}\right)\right), \quad (3)$$

where Nc is the density of states in the conduction band, and $G_{\frac{1}{2}}$ is the inverse Fermi function of order 1/2 defined with

$$G_{\frac{1}{2}}\left(\frac{2}{\pi}\cdot F^{\alpha}_{\frac{1}{2}}(x)\right) = x. \quad (4)$$

The carrier density n including nonparabolic band effects is given by [18]

$$n = N_c\frac{2}{\pi}F^{\alpha}_{\frac{1}{2}}(\eta) = N_c\frac{2}{\pi}\int_0^{\infty}\frac{(1+2\alpha\epsilon)\sqrt{\epsilon(1+\alpha\epsilon)}}{1+\exp(\epsilon-\eta)}d\epsilon, \quad (5)$$

where $\eta = (E_f - E_c)/kT$ is the normalized Fermi level. The parameter α is a coefficient of nonparabolicity that can be calculated as

$$\alpha = \frac{1}{\epsilon_g}\left(1 - \frac{m}{m_0}\right)^2, \quad (6)$$

where ϵ_g is the normalized band gap $(= E_c - E_v/kT)$ and m_0 is the free electron rest mass. The simple analytical approximation of the inverse Fermi function is given in [19] for a weak degenerate case ($\eta < 10$). For high η, we apply Sommerfeld's approximation to calculate the inverse Fermi function. Both approximations are linearly interpolated.

By employing the expression (1) in the QET model, we obtain the current density

$$J_n = q\mu_n\left(\nabla\left(n\frac{kT_n}{q}\right) - n\nabla(\varphi + \gamma_n + \omega_n)\right), \quad (7)$$

where μ_n is the electron mobility. From (2), the quantum potential equation is obtained as

$$2b_n\nabla^2\rho_n - \gamma_n\rho_n = 0, \quad (8)$$

where $b_n = \frac{\hbar^2}{12qm}$. The root-density ρ_n is written as $\rho_n = \sqrt{n} = \sqrt{n_i}exp(u_n)$ by a variable $u_n = \frac{q}{kT_n}(\frac{(\varphi+\gamma_n+\omega_n-\varphi_n)}{2})$ in (1). As shown in [16], under Fermi–Dirac statistics, (8) is replaced by the equivalent form

$$b_n\nabla\cdot(\rho_n\nabla u_n) - \frac{kT_n}{q}\rho_n u_n = -\frac{\rho_n}{2}(\varphi + \omega_n - \varphi_n). \quad (9)$$

If the variable u_n is uniformly bounded, the electron density is maintained to be positive. This approach provides a numerical advantage for developing an iterative solution method.

For electrons, the four-moments QET model based on Fermi–Dirac statistics is described as follows:

$$\epsilon\Delta\varphi = q(n - p - C_{imp}), \quad (10)$$

$$\frac{1}{q}divJ_n = 0, \quad (11)$$

$$J_n = q\mu_n\left(\nabla\left(n\frac{kT_n}{q}\right) - n\nabla(\varphi + \omega_n + \gamma_n)\right), \quad (12)$$

$$b_n\nabla\cdot(\rho_n\nabla u_n) - \frac{kT_n}{q}\rho_n u_n = -\frac{\rho_n}{2}(\varphi + \omega_n - \varphi_n), \quad (13)$$

$$\nabla\cdot S_n = -J_n\cdot\nabla\varphi - \frac{3}{2}kn\frac{T_n - T_L}{\tau_\epsilon}, \quad (14)$$

$$S_n = -\frac{\mu_s}{\mu_n}\left(\frac{5}{2}\frac{kT_n}{q} - \frac{\hbar^2}{24mq}\Delta\log n - \gamma_n\right)J_n - \frac{\mu_s}{\mu_n}\frac{5}{2}\left(\frac{k}{q}\right)^2 q\mu_n nT_n\nabla T_n, \quad (15)$$

Table 1 Parameters for the low-field mobility model

Material	Si [25]	Ge [25]	$In_{0.53}Ga_{0.47}As$ [26]
$\mu_L (cm^2/Vs)$	1400	3900	14000
$\mu_{min} (cm^2/Vs)$	80	850	300
C_{ref}	1.12e17	2.6e17	1.3e17
α_{LF}	0.72	0.56	0.48

where p, ϵ and C_{imp} are the hole density, the permittivity of semiconductor, and the ionized impurity density, respectively. T_L and τ_ϵ are the lattice temperature and energy relaxation time. The ratio μ_n/μ_s selected here is 0.8 [20]. For holes, similar expressions are obtained.

2.2 Mobility model

For the energy dependence of the mobility, we apply the model of the Baccarani et al. [21],

$$\frac{\mu_n(T_n)}{\mu_{LF}} = \frac{T_L}{T_n}. \tag{16}$$

In the homogeneous case, this model is equivalent to the Hänsch mobility model [20]

$$\frac{\mu_n(T_n)}{\mu_{LF}} = \left(1 + \frac{3}{2}\frac{\mu_{LF} k}{q\tau_\epsilon v_s^2}(T_n - T_L)\right)^{-1}, \tag{17}$$

where v_s is the saturation velocity. As mentioned in [22,23], the Hänsch mobility model is consistent with the high-field mobility model

$$\frac{\mu_n(E)}{\mu_{LF}} = \frac{1}{\xi + \left((1-\xi)^\beta + \left(\frac{\mu_{LF}\cdot E}{v_{sat}}\right)^\beta\right)^{\frac{1}{\beta}}} \tag{18}$$

with the parameters $\xi = 1/2$ and $\beta = 2$.

To account for the mobility reduction due to the ionized impurity scattering, we use the formula of Caughey and Thomas [24] for the low-field mobility μ_{LF} in this work:

$$\mu_{LF} = \mu_{min} + \frac{\mu_L - \mu_{min}}{1 + \left(\frac{C}{C_{ref}}\right)^{\alpha_{LF}}}. \tag{19}$$

The model parameter values [25,26] are summarized in Table 1. In this work, numerical simulations are performed by using the Baccarani's mobility model (16) for the QET model and the high-field mobility model (18) for the QDD model, respectively. The effects of interface traps and surface roughness scattering are not included in this work.

3 Simulation results

3.1 Device structures

The schematic views of simulated devices are shown in Fig. 1. Si, Ge, and $In_{0.53}Ga_{0.47}As$ n-MOSFETs with high-k/metal gates are examined. Selected material parameters are listed in Table 2. The relative dielectric permittivity considered here is 22, and the value is known as "HfO_2". The equivalent oxide thickness (EOT) is 0.6 nm. The threshold of all devices is obtained by the adjustment of the gate work function, which is selected for each semiconductor material to meet a common threshold voltage of 0.2 V. The threshold voltage is defined as the gate voltage when the drain current is 10 µA/µm. The channel length of simulated devices is varied from 35 to 16 nm. The S/D doping is N_{SD} =

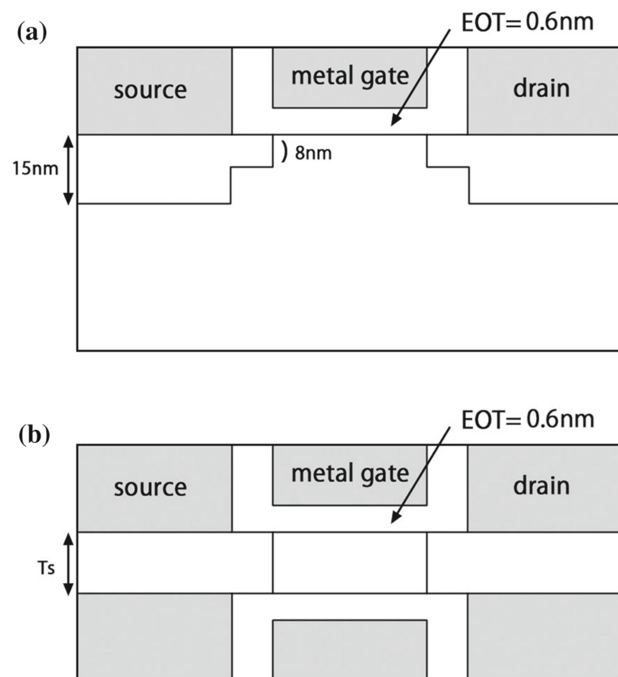

Fig. 1 Schematic views of simulated (**a**) Bulk and (**b**) DG MOSFETs. The channel length is varied from 35 to 16 nm

Table 2 Selected semiconductor material parameters

Semiconductor	Si	Ge	$In_{0.53}Ga_{0.47}As$
$E_G(eV)$	1.12 [6]	0.66 [6]	0.73 [6]
$\epsilon_R(\epsilon_0)$	11.7 [6]	16.0 [6]	14.0 [6]
$m_{eff}(m_0)$	0.26 [29]	0.12 [29]	0.048 [6]
$n_i(cm^{-3})$	1.08e10 [29]	1.64e13 [29]	9.0e11 [28]
v_{sat} (cm/s)	1.0e7 [27]	0.7e7 [27]	0.75e7 [27]
$N_{SD}(cm^{-3})$	1.0e20	1.0e20	2.0e19 [2]
$N_c(cm^{-3})$	2.86e19	1.05e19	2.64e17

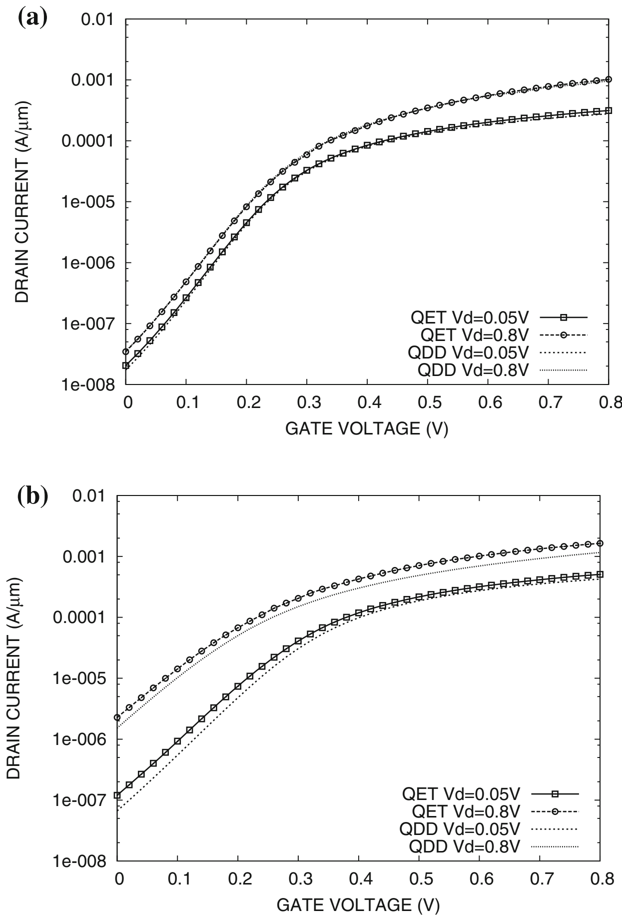

Fig. 2 Comparison of the I_d–V_G characteristics of Si bulk n-MOSFETs between QET and QDD models. **a** Lg = 50 nm, **b** Lg = 20 nm

1.0×10^{20} cm^{-3} for Si and Ge n-MOSFETs. Since activated donor concentrations larger than 2.0×10^{19} cm^{-3} cannot be obtained in $In_{0.53}Ga_{0.47}As$ n-MOSFETs [2], we set up $N_{SD} = 2.0 \times 10^{19}$ cm^{-3} for an $In_{0.53}Ga_{0.47}As$ n-MOSFET. We further assume channel dopings of 2.0×10^{18} cm^{-3} for bulk n-MOSFETs, and 1.0×10^{15} cm^{-3} for double-gate n-MOSFETs.

3.2 QET simulations

Figure 2a and b demonstrates the I_D– V_G characteristics of 50 and 20 nm Si bulk n-MOSFETs at $V_d = 0.05$V and 0.8 V, which are calculated by the QET and QDD models. The same work function is used for both models. In a long channel device, the I_D–V_G characteristics calculated by two models are almost identical, as shown in Fig. 2a. For the ultra-short channel device, two models exhibit the different results of I_D–V_G characteristics due to the non-local transport effects and the reduction of the quantum confinement effects. The QET model provides higher drain current. The subthreshold slope (SS) calculated by the QET model is increased from 107 mV/dec to 114 mV/dec. Figure 3 shows the average distance of electrons from the interface calculated by the QET and QDD models. The simulations are done at $V_g = 0.8$ V and $V_d = 0.8$ V. The hot electron effects result in the spread

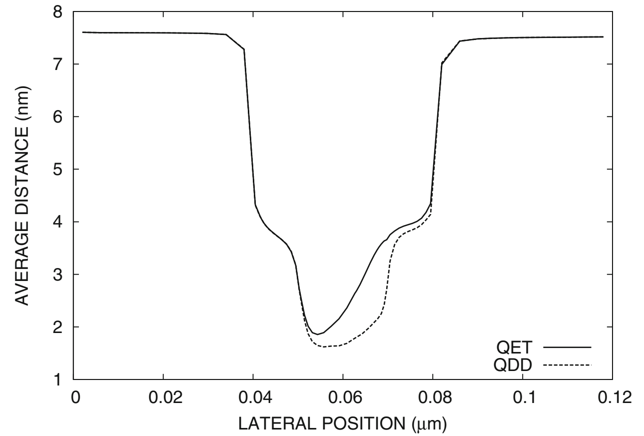

Fig. 3 Comparison of the average distance of carriers from interface for a 20 nm Si bulk n-MOSFET between QET and QDD models

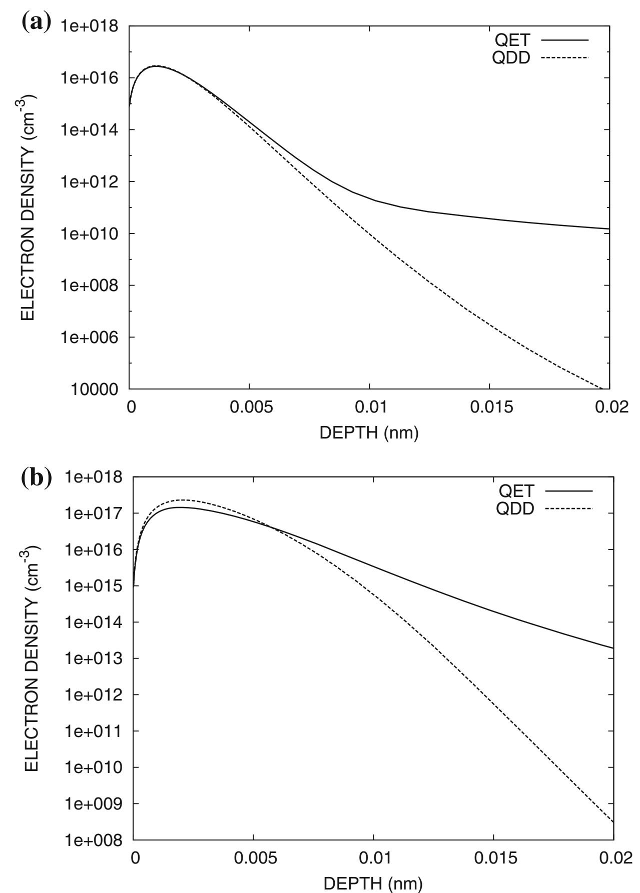

Fig. 4 Electron density distributions perpendicular to the interface for Si bulk n-MOSFETs calculated by QET and QDD models at the center of the channel. Vg = 0.1 V, Vd = 0.8 V. **a** Lg = 50 nm, **b** Lg = 20 nm

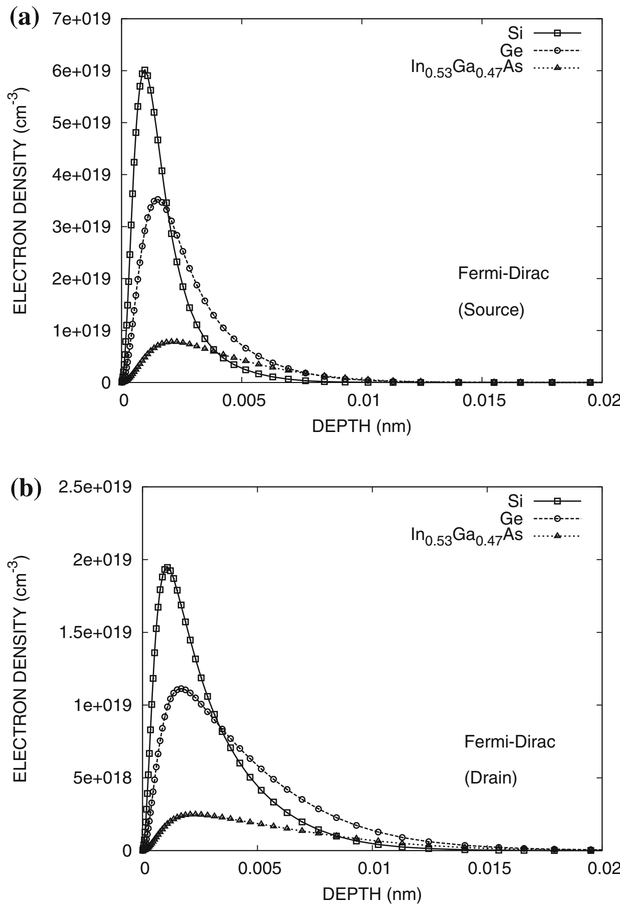

Fig. 5 Electron density distributions perpendicular to the interface for 20 nm Si, Ge, and $In_{0.53}Ga_{0.47}As$ bulk n-MOSFETs calculated by the QET model based on Fermi–Dirac statistics. **a** at the source end of the channel, **b** at the drain end of the channel. $V_g = 0.8$ V, $V_d = 0.8$ V

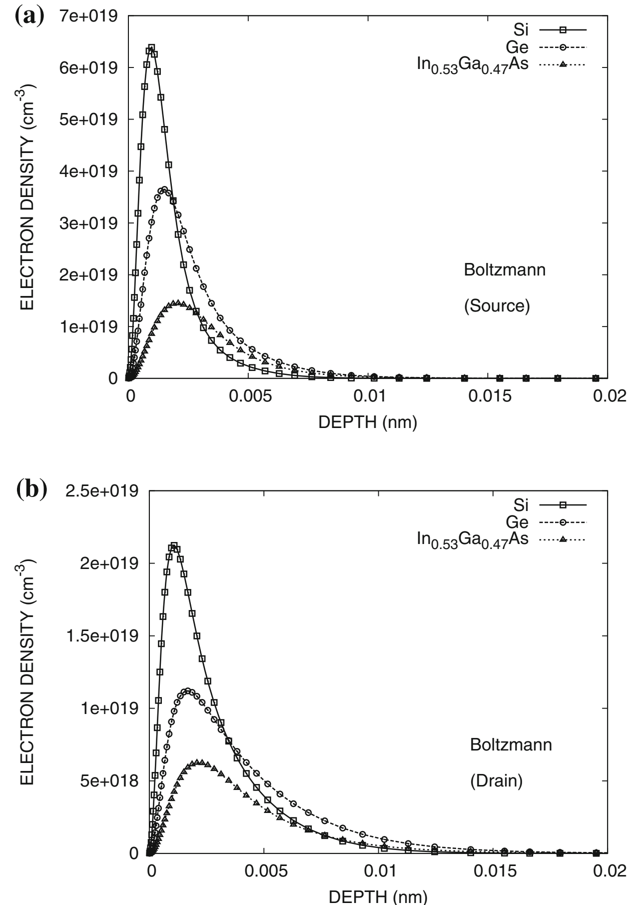

Fig. 6 Electron density distributions perpendicular to the interface for 20 nm Si, Ge, and $In_{0.53}Ga_{0.47}As$ bulk n-MOSFETs calculated by the QET model based on Boltzmann statistics. **a** at the source end of the channel, **b** at the drain end of the channel. $V_g = 0.8$ V, $V_d = 0.8$ V

of electrons toward the bulk in the channel and hence in ultra-short channel devices, a significant difference between two models is induced. The results clearly indicate that the quantum confinement effect in the ultra-short channel is reduced by the enhanced diffusion due to the high electron temperature. Figure 4a and b shows the electron density distributions calculated by the QET and QDD models for long and short channel devices. The results are plotted at the center of the channel. In the long channel device, the electron density distributions calculated by two models are almost identical at the surface. For the ultra-short channel device, due to the hot carrier effects, the electron density distribution calculated by the QET model is spread towards the bulk. This result in the reduction of charge control calculated by the QET model.

3.3 Quantum confinement effects

The dependence of quantum confinement effects on channel materials is investigated in Figs. 5 and 6. The results under Fermi–Dirac statistics and Boltzmann statistics are compared. The electron density distributions for 20 nm Si, Ge and $In_{0.53}Ga_{0.47}As$ bulk n-MOSFETs are plotted at the source and drain ends of the channel. The devices are simulated at $V_g = 0.8$ V and $V_d = 0.8$ V. As shown in Fig. 5a, the inversion layer electrons in Ge and $In_{0.53}Ga_{0.47}As$ n-MOSFETs spread into the bulk at the source end of the channel due to the low effective mass and high permittivity. Figure 5b reveals that in all devices the quantum confinement effect is further reduced by the enhanced diffusion due to the high electron temperature. These properties degrade the short channel effects of Ge and $In_{0.53}Ga_{0.47}As$ devices when compared with Si devices, as discussed later. Since $N_c (= 2.64 \times 10^{17}\ \text{cm}^{-3})$ of $In_{0.53}Ga_{0.47}As$ is low, the inversion layer electrons in the $In_{0.53}Ga_{0.47}As$ n-MOSFET are further decreased due to the high degeneracy material.

In Fig. 7a and b, we compare the electron density distributions calculated by the QET model based on Fermi-Dirac statistics for 20 nm Si, Ge, and $In_{0.53}Ga_{0.47}As$ double-gate n-MOSFETs, respectively. The double-gate structures having a film thickness of 8 nm are simulated. The results are plot-

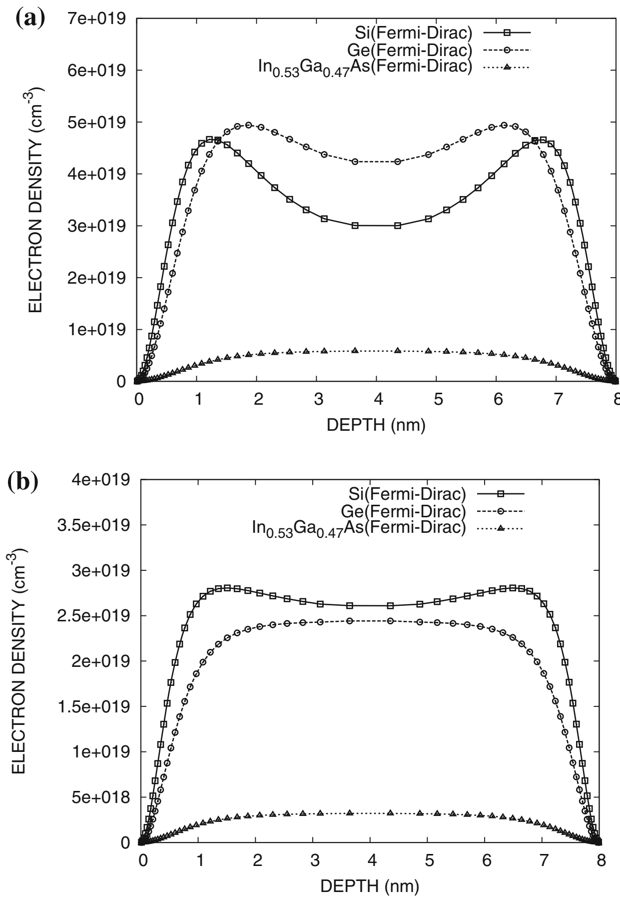

Fig. 7 Electron density distributions perpendicular to the interface for 20 nm Si, Ge, and $In_{0.53}Ga_{0.47}As$ doube gate n-MOSFETs calculated by the QET model based on Fermi–Dirac statistics. **a** at the source end of the channel, **b** at the drain end of the channel. $V_g = 0.8$ V, $V_d = 0.8$

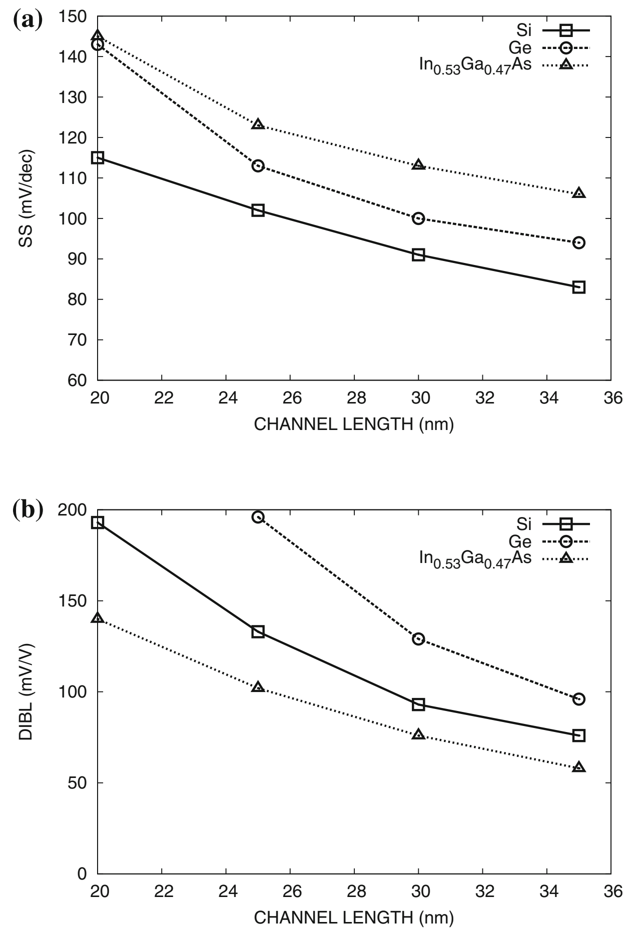

Fig. 8 **a** Subthreshold slope at $V_d = 0.05$V versus channel length of Si, Ge, and $In_{0.53}Ga_{0.47}As$ bulk n-MOSFETs. **b** Drain-induced barrier lowering versus channel length of bulk Si, Ge, and $In_{0.53}Ga_{0.47}As$ n-MOSFETs

ted at the source and drain ends of the channel. The devices are simulated at $V_g = 0.8$ V and $V_d = 0.8$ V. The inversion layer electrons in Ge and $In_{0.53}Ga_{0.47}As$ n-MOSFETs spread into the center of the channel due to the low effective mass and high permittivity. In analogy to the results of bulk n-MOSFETs, the single inversion layer electrons in the $In_{0.53}Ga_{0.47}As$ n-MOSFET are further decreased due to the high degeneracy material. In Fig. 7a, Si and Ge n-MOSFETs exhibit two inversion layers at the source end of the channel. In the film thickness of 8 nm, Ge n-MOSFETs form a single inversion layer due to the hot electron effects at the drain end of the channel as shown in Fig. 7b.

3.4 Short channel effects

Figure 8a and b indicates the SS and DIBL as a function of the channel length for Si, Ge, and $In_{0.53}Ga_{0.47}As$ bulk n-MOSFETs. The simulations are performed by using the QET model based on Fermi–Dirac statistics. As seen in Fig. 8a, the SS of Ge and $In_{0.53}Ga_{0.47}As$ n-MOSFETs is larger than that of the Si n-MOSFET due to smaller electron effective mass and higher permittivity. It is shown in Fig. 8b that the DIBL of $In_{0.53}Ga_{0.47}As$ n-MOSFET is suppressed because of the low S/D doping concentration. Fig. 9a and b shows the dependence of SS and DIBL on the channel length for Si, Ge, and $In_{0.53}Ga_{0.47}As$ double-gate n-MOSFETs. The short channel effects are suppressed in the multi-gate structure. A different improvement between SS and DIBL is seen. In all devices, the DIBL effect is reduced in double-gate n-MOSFETs. In the $In_{0.53}Ga_{0.47}As$ n-MOSFET, the DIBL effect is significantly reduced due to the low S/D doping concentration. This is because the thin film suppresses an extension of drain electric field into the channel. The SS improvement depends on the channel material even in double gate structure. The SS of Ge and $In_{0.53}Ga_{0.47}As$ n-MOSFETs are larger than that of Si n-MOSFET due to the low effective mass and high permittivity as well as the results of bulk n-MOSFETs. Figure 10 shows the threshold voltage roll-off of Si, Ge, and $In_{0.53}Ga_{0.47}As$ n-MOSFETs at $V_d = 0.5\ V$. The results of

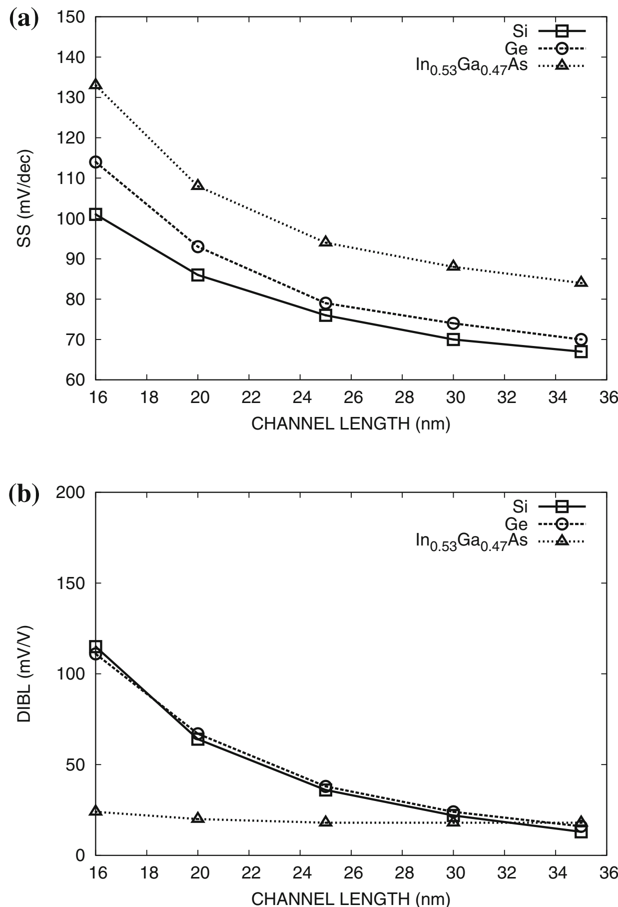

Fig. 9 **a** Subthreshold slope at $V_d = 0.05$V versus channel length of Si, Ge, and $In_{0.53}Ga_{0.47}As$ double-gate n-MOSFETs. **b** Drain-induced barrier lowering versus channel length of Si, Ge, and $In_{0.53}Ga_{0.47}As$ double-gate n-MOSFETs

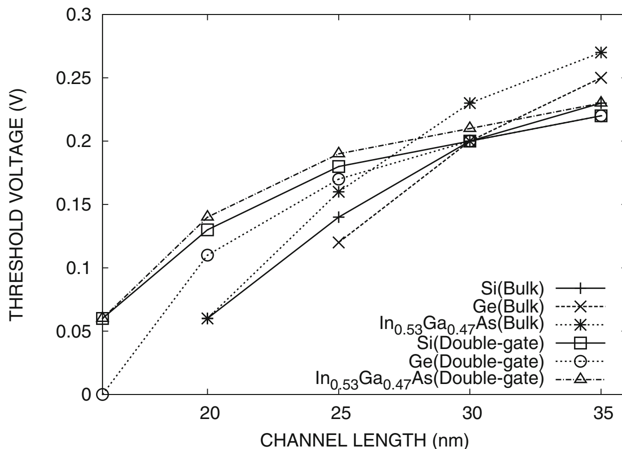

Fig. 10 Threshold voltage roll-off at $V_d = 0.5$ V versus channel length of Si, Ge, $In_{0.53}Ga_{0.47}As$ bulk and double-gate n-MOSFETs.

both bulk and double-gate n-MOSFETs are shown. The V_T roll-off of the $In_{0.53}Ga_{0.47}As$ n-MOSFET is almost the same as that of Si n-MOSFET in the double gate structure because of the low S/D doping concentration. The Ge n-MOSFET shows the worst short channel effects.

4 Conclusion

The quantum confinement and short channel effects of Si, Ge, and $In_{0.53}Ga_{0.47}As$ n-MOSFETs have been evaluated using a 4-moments QET model based on Fermi–Dirac statistics and nonparabolicity. The dependence of quantum confinement effects on channel materials has been clarified. The charge control by the gate is reduced in Ge and $In_{0.53}Ga_{0.47}As$ n-MOSFETs due to the low effective mass and high permittivity. This results in the degradation of short channel effects. The double-gate structure is effective in the suppression of DIBL for all channel materials. The SS degradation depends on channel materials even in double-gate structure.

Open Access This article is distributed under the terms of the Creative Commons Attribution 4.0 International License (http://creativecommons.org/licenses/by/4.0/), which permits unrestricted use, distribution, and reproduction in any medium, provided you give appropriate credit to the original author(s) and the source, provide a link to the Creative Commons license, and indicate if changes were made.

References

1. Bohr, M.: The evolution of scaling from the homogeneous era to the heterogeneous era. In: Proceedings of IEDM, pp. 1.1.1–1.1.6 (2011)
2. Fischetti, M.V., Laux, S.E.: Monte Carlo simulation of transport in technologically significant semiconductors of the diamond and Zinc-Blende structures-Part II: submicrometer MOSFET's. IEEE Trans. Electron Devices **38**, 650–660 (1991)
3. Hisamoto, D., Lee, W.-C., Kedzierski, J., Takeuchi, H., Kuo, C., Anderson, E., King, T.-J., Bokor, J., Hu, C.: FinFET-A self-aligned double-gate MOSFET scalable to 20 nm. IEEE Trans. Electron Devices **47**, 2320–2325 (2000)
4. Singh, N., Agrwal, A., Bera, L.K., Liow, T.Y., Yang, R., Rustagi, S.C., Tung, C.H., Kumer, R., Lo, G.Q., Balasubramanian, N., Kwong, D.L.: High-performance fully depleted silicon nanowire (diameter $\leq$ 5nm) gate-all-around CMOS devices. IEEE Electron Device Lett. **27**, 383–386 (2006)
5. Fischetti, M.V., O'Regan, T.P.: Theoretical study of some physical aspects of electronic transport in nMOSFETs at the 10-nm gate-length. IEEE Trans. Electron Devices **54**, 2116–2136 (2007)
6. Laux, S.E.: A simulation study of the switching times of 22- and 17-nm gate-length SOI nFETs on high mobility substrates and Si. IEEE Trans. Electron Devices **54**, 2304–2320 (2007)
7. Lizzit, D., Esseni, D., Palestri, P., Osgnach, P., Selmi, L.: Performance benchmarking and effective channel length for nanoscale InAs, $In_{0.53}$ $Ga_{0.47}As$, and sSi n-MOSFETs. IEEE Trans. Electron Devices **61**, 2027–2034 (2014)
8. Park, S.H., Liu, Y., Kharche, N., Jelodar, M.S., Klimeck, G., Lundstrom, M.S., Luisier, M.: Performance comparisons of III-V and strained-Si in planar FETs and nonplanar FinFETs at ultrashort gate length(12nm). IEEE Trans. Electron Devices **59**, 2107–2114 (2012)

9. Moreau, M., Munteanu, D., Autran, J.L.: Simulation study of short-channel effects and quantum confinement in double-gate FinFET devices with high-mobility materials. Microelectron. Eng. **88**, 366–369 (2011)
10. Mori, T., Asuma, Y., Tsuchiya, H., Miyoshi, T.: Comparative study on drive current of III-V semiconductor, Ge and Si channel n-MOSFETs based on quantum-corrected Monte Carlo simulation. IEEE Trans. Nanotechnol. **7**, 237–241 (2008)
11. Luisier, M.: Performance comparison of GaSb, strained-Si, and InGaAs double-gate ultra-thin-body n-FETs. IEEE Electron Devices **32**, 1686–1688 (2011)
12. Gardner, C.L.: The quantum hydrodynamic model for semiconductor devices. SIAM J. Appl. Math. **54**, 409–427 (1994)
13. Sho, S., Odanaka, S.: A quantum energy transport model for semiconductor device simulation. J. Comput. Phys. **235**, 486–496 (2013)
14. Gritsch, M., Kosina, H., Grasser, T., Selberherr, S.: Revision of the standard hydrodynamic transport model for SOI simulation. IEEE Trans. Electron Devices **49**, 1814–1820 (2002)
15. O'Regan, T.P., Hurley, P.K., Soree, B., Fischetti, M.V.: Modeling the capacitance-voltage response of $In_{0.53}Ga_{0.47}As$ metal-oxide-semiconductor structures: Charge quantization and nonparabolic corrections. Appl. Phys. Lett. **96**, 213514 (2010)
16. Odanaka, S.: Multidimensional discretization of the stationary quantum drift-diffusion model for ultrasmall MOSFET structures. IEEE Trans. CAD ICAS **23**, 837–842 (2004)
17. Sho, S., Odanaka, S., Hiroki, A.: A Fermi-Dirac statistics based quantum energy transport model for high mobility MOSFETs. JASSE **2**, 153–170 (2015)
18. Bebb, H.B., Ratliff, C.R.: Numerical tabulation of integrals of Fermi functions using $\mathbf{k} \cdot \mathbf{p}$ density of states. J. Appl. Phys. **42**, 3189–3194(1971)
19. Altschul, V., Finkman, E.: Simple approximation for Fermi energy in nonparabolic semiconductors. Appl. Phys. Lett. **58**, 942–944 (1991)
20. Grasser, T., Tang, T.-W., Kosina, H., Selberherr, S.: A review of hydrodynamic and energy-transport models for semiconductor device simulation. IEEE Proc. **91**(2), 251–274 (2003)
21. Baccarani, G., Wordeman, M.R.: An investigation of steady-state velocity overshoot in silicon. Solid-State Elec. **28**, 407–416 (1985)
22. Grasser, T., Kosina, H., Selberherr, S.: Consistent comparison of drift diffusion and hydrodynamic device simulations. In: Proceedings of SISPAD, pp. 151-154 (1999)
23. Hänsch, W., Miura-Mattausch, M.: The hot-electron problem in small semiconductor devices. J. Appl. Phys. **60**, 650–656 (1986)
24. Caughey, D.M., Thomas, R.E.: Carrier mobilities in silicon empirically related to doping and field. Proc. IEEE **52**, 2192–2193 (1967)
25. Selberherr, S.: Analysis and Simulation of Semiconductor Devices. Springer, Wien (1984)
26. Sotoodeh, M., Khalid, A.H., Rezazadeh, A.A.: Empirical low-field mobility model for III-V compounds applicable in device simulation codes. J. Appl. Phys. **87**, 2890–2900 (2000)
27. Quey, R., Moglestue, C., Palankovski, V., Selberherr, S.: A temperature dependent model for the saturation velocity in semiconductor materials. Mater. Sci. Semicond. Process. **3**, 149–155 (2000)
28. Carmody, C., Tan, H.H., Jagadish, C., Gaarder, A.: Ion-implanted In0.53Ga0.47As for ultrafast optoelectronic applications. Appl. Phys. Lett. **82**, 3913–3915 (2003)
29. Anderson, B.L., Anderson, R.L.: Fundamentals of Semiconductor Devices. In: Paulson, C (ed.) McGraw-Hill, New York (2005)